Supporting Information

Co-assembly of Photosystem II/Reduced Graphene Oxide Multilayered Biohybrid Films for Enhanced Photocurrent

Peng Cai[a], Xiyun Feng[a], Jinbo Fei[a], Guangle Li[a], Jiao Li[a,b], Huang Jianguo[b] and Junbai Li*[a]

[a]Beijing National Laboratory for Molecular Sciences (BNLMS), CAS Key Lab of Colloid, Interface and Chemical Thermodynamics, Institute of Chemistry, Chinese Academy of Sciences, Beijing 100190, China.

E-mail: jbli@iccas.ac.cn

[b]Department of Chemistry, Zhejiang University, Hangzhou, Zhejiang 310027, China.

Section I. Synthesis of GO and PEI-rGO

GO sheets were synthesized from natural graphite powder using a modified Hummers method.[1] Typically, 3.0 g graphite powder was added to 70 mL of concentrated H_2SO_4 (98%) and stirred at room temperature. 1.5 g $NaNO_3$ was added and the mixture solution was kept in an ice bath. With vigorously stirring, 9.0 g $KMnO_4$ was added very slowly to keep the temperature below 10 °C. After stirred for 2 h, the mixture was put at room temperature and kept stirring for another 5 days. Then, 140 mL of deionized (DI) water was added to the mixture and stirred for 15 min. Afterwards the mixture solution was further diluted by 500 mL of DI water under vigorous stirring. 20 mL of H_2O_2 (30%, wt) was then added to the mixture and the color of the solution changed from dark brown to brilliant yellow with bubbling. The mixture was centrifuged and washed with 1:10 HCl/water solution (250 mL) and DI water by centrifugation until the pH of the suspensions was between 6 and 7. Finally, the product was dialyzed for 1 week to remove impurity atoms and then freeze-dried until further use.

For the reduction of GO with PEI, 0.25 mg mL^{-1} GO sheets were dispersed in water and ultra-sonicated for 30 min. The resultant aqueous GO dispersion (40 mL) was mixed with 40 mL of 4 mg mL^{-1} PEI aqueous solution, and the mixed solution was then stirred at 60 °C for 12 h. After cooled to room temperature, 120 μL of hydrazine monohydrate (85%) solution was added to the resulting dispersion. After being vigorously shaken, the reaction system was put in an oil bath at 95 °C for 12 h. After reaction, extra PEI and hydrazine hydrate were removed by repeated centrifugation at 14,000 rpm for 10 min, washed three times, and followed by redispersing in DI water for further use.

Section II. Purification of PSII enriched membranes from commercially available baby spinach

PSII enriched membranes were isolated and purified from spinach chloroplasts, according to reported methods with modifications.[2,3] All the following steps were carried out at 4 °C. About 200 g of spinach leaves were washed and kept overnight. Together with 400 mL of buffer A (20 mM Tricine-NaOH pH 7.8, 0.4 M sucrose, 2 mM $MgCl_2$, 40 mM NaCl, 2 mM Vitamin C, 0.2% bovine serum albumin (BSA)), the stored spinach leaves were homogenized in a precooled blender and filtered with eight layers of cotton gauze. The obtained filtrate was centrifuged at 400 g for 1 min and chloroplasts were collected by centrifuging the supernatant at 6000 rpm for 15

min. To break the chloroplasts and remove water soluble proteins from the outer surface of the thylakoid membranes, the precipitant was suspended in hypotonic buffer B (20 mM Tricine-NaOH pH 7.8, 5 mM $MgCl_2$, 10 mM NaCl, 0.2% BSA) and stirred for 15 min. Following 2 min of centrifugation at 250 g, the resulting supernatant was collected and centrifuged at 7,000 g for 15 min to get thylakoid membranes. After suspending the pellet in a high ionic strength buffer C (20 mM MES-NaOH pH 6.5, 0.4 M sucrose, 15 mM NaCl, 5 mM $MgCl_2$), the volume of suspension was measured, and the chlorophyll (Chl) concentration was then determined according to literature[1] and adjusted to 2.5 mg Chl mL^{-1} by adding buffer C. Buffer D (buffer C containing an additional 20 wt% TX-100) was slowly added to the suspension with gently stirring to avoid foaming until the ratio of TX-100 to Chl (w/w) is 20:1. After stirring for 10 min, the suspension was centrifuged at 10,000 g for 1 min to remove starch grains and debris, and then centrifuged at 35,000 g for 30 min. The above precipitate was washed with buffer C repeatedly until the supernatant is colorless. The final product was resuspended in 5 mL buffer E (buffer C containing an additional 0.5 M betaine), and frozen in liquid nitrogen in 0.5 mL aliquots after the Chl concentration was determined.

Section III. Layer-by-Layer Self-assembly of the PEI/PSII and PEI-rGO/PSII multilayered films

The ITO substrates were cut into 6 × 25 mm rectangular pieces, the effective area (coating area) of the electrode is 0.42 cm^2, cleaned in an ethanol solution and sonicated for 30 min, then rinsed with DI water, and dried with a stream of N_2. Positively charged PEI or PEI-rGO was first absorbed on the substrates by immersing these substrates into PEI (2.0 mg mL^{-1}, 0.2 M NaCl, 20 mM MES, pH 6.5) or PEI-rGO (0.25 mg mL^{-1}) solution for 30 min, respectively. Then, after washing three times with MES buffer (20 mM, pH 6.5), followed by drying with a gentle stream of N_2, the resultant substrates were immersed in PSII solution (0.5 mg Chl mL^{-1} 20 mM MES) for 30 min, rinsed with MES, and dried by a stream of N_2. Thus, one bilayer was obtained, named $(PEI/PSII)_1$ and $(PEI\text{-}rGO/PSII)_1$, respectively. This process was repeated until the desired number of layers was obtained. The above samples were used for photocurrent and UV-vis spectrophotometry measurements. The AFM and SEM samples were further washed three times with DI water and dried by a stream of N_2. As a comparison, pure PSII and PEI-rGO film were prepared by the application of certain amount of PSII and PEI-rGO solution on the electrode

surface with controlled areas (0.42 cm^2) and dried without washing. All the above assembly processes were performed at 4 °C.

For dried films on ITO substrate, UV-vis absorption spectra were applied both before and after the photocurrent measurements and no significant absorbance difference was found.

Section IV. Photocurrent Measurements

The coated ITO glass was used as the working electrode, a saturated calomel electrode (SCE) as the reference electrode, and a platinum wire as the counter electrode. A home-built system that included a Xe lamp (P = 150 W) with two filters ($\lambda > 550$ nm and $\lambda < 800$ nm) and a condenser was used for light irradiation. The power density at 680 nm is 10 mW cm^{-2}. A buffer contained 20 mM MES, 50 mM KCl, 5 mM $MgCl_2$ and 3 mM $CaCl_2$ was used as the electrolyte for the photocurrent measurement of direct electron transfer and the stability test. Before irradiation, the solution was bubbled with N_2 for at least 1 h to eliminate dissolved O_2 and the whole experimental process was conducted under N_2 protection.

According to the precious report,[4] the quantum efficiencies of different photoanodes were calculated using the following modified equation:

$$\varphi(\%) = \{1240 \times j\ (\mu A\ cm^{-2})\} / \{P\ (W\ m^{-2}) \times \lambda\ (nm) \times (1-T)\}$$

where j, P, λ and T indicate a photocurrent density, the incident photon flux (100 W m^{-2}), the wavelength of the incident light (680 nm) and the transmissivity of the electrode, respectively. In this case, the photons reflected and absorbed by electrolytic cell were not taken into consideration.

The photocurrent action spectrum of PSII on ITO substrate was measured using different band pass filters (half-width: 10 nm) with the power at corresponding central wavelength adjusted to 350 μW cm^{-2}. 1 mM 2,5-dichloro-1,4-benzoquinone was added in the electrolyte to enhance the photocurrent signal. Considering the electron acceptor is photo-responsive in the cyan region, we could just give the photocurrent action spectrum between 490 and 700 nm.

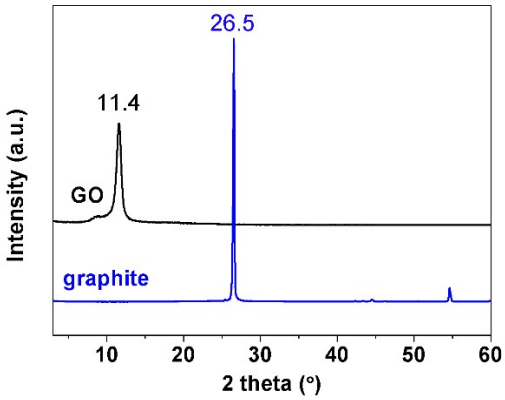

Figure S1. X-ray diffraction patterns of graphite powder (blue curve) and GO powder (black curve).

The diffraction peak at 11.4° corresponds to GO (001) with interlayer spacing of around 0.8 nm, which is larger than that of natural graphite (26.5°) suggesting efficient oxidation of graphite.

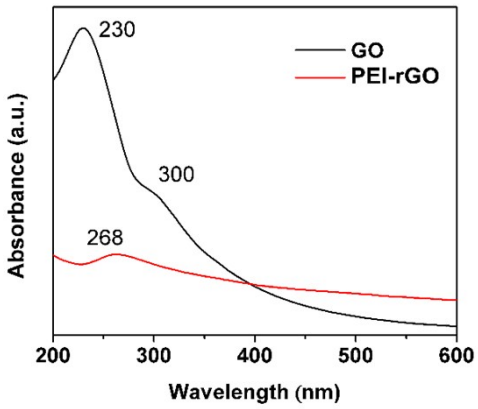

Figure S2. UV-vis spectra of GO (black curve) and PEI-rGO (red curve) dispersed in aqueous solution.

The absorbance peaks at 230 and 300 nm, characteristic of GO, shifted to 268 nm. Meanwhile, the intensity of the absorption tail in the visible region (>300 nm) increased, which means that PEI-rGO sheets uniformly disperse in aqueous solution.

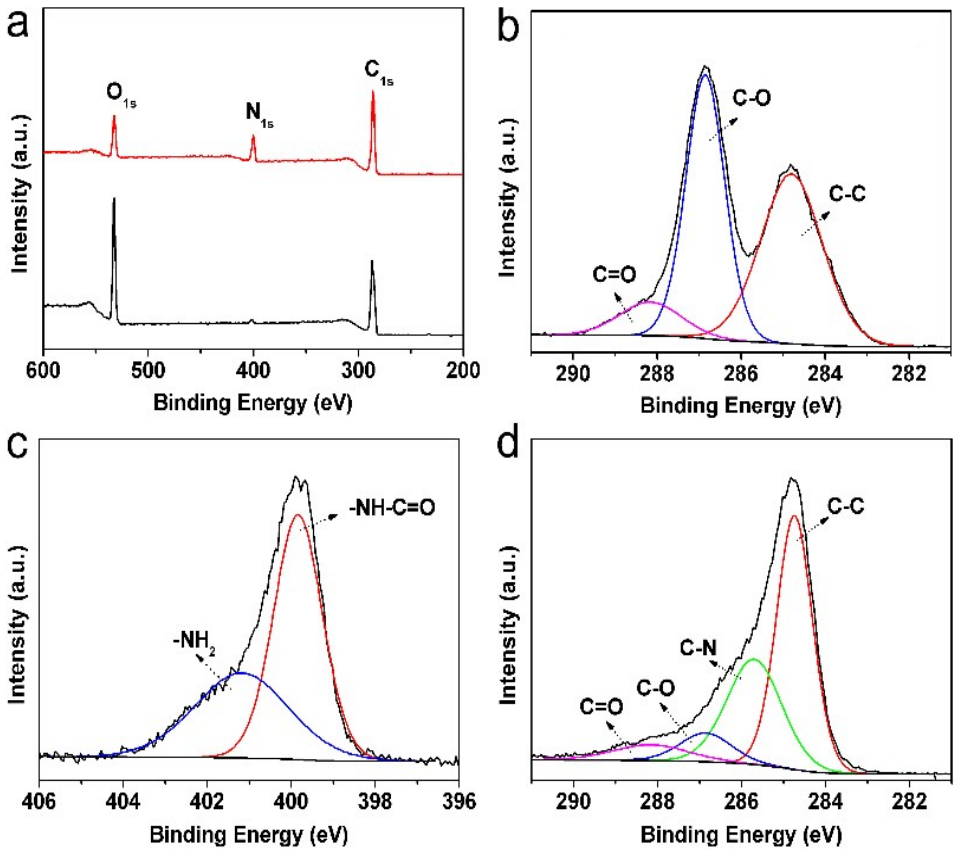

Figure S3. XPS spectra of GO and PEI-rGO. (a) Wide scan survey spectra of GO (black curve) and PEI-rGO (red curve); (b) C1s spectrum of GO; (c) N1s spectrum of PEI-rGO; and (d) C1s spectrum of PEI-rGO.

As shown in Figure S3a, the survey spectrum of PEI-rGO shows an intensified nitrogen peak at ~399 eV and a decreased oxygen peak at ~530 eV as compared to that of GO, implying the efficient adhesion of the PEI chain on the graphene surfaces and considerable removal of oxygen-containing functional groups. Meanwhile, the C1s XPS spectrum of GO (Figure S3b) shows pronounced peaks at 286.7 and 288.2 eV, attributable to C-O and C=O bonds, respectively. However, the corresponding peaks in the C1s spectrum of PEI-rGO decrease significantly (Figure S3d). Furthermore, the N1s XPS spectrum of PEI-rGO in Figure S3c implies the presence of amine NH_2 (401.2 eV) and amide bonds N-C=O (399.8 eV), suggesting some of the PEI chains have been covalently linked to the graphene surface via the formation of amide bonds.

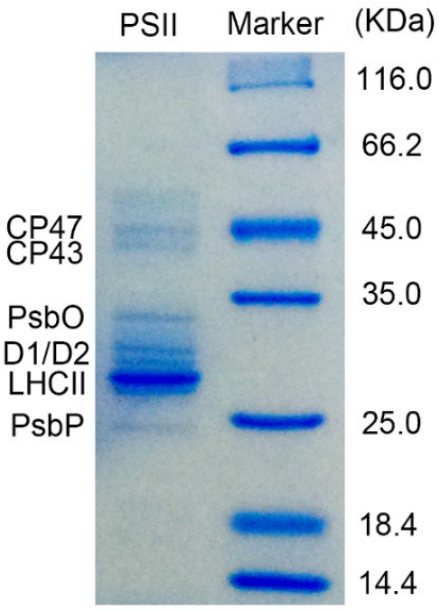

Figure S4. SDS-PAGE patterns of PSII enriched membranes.

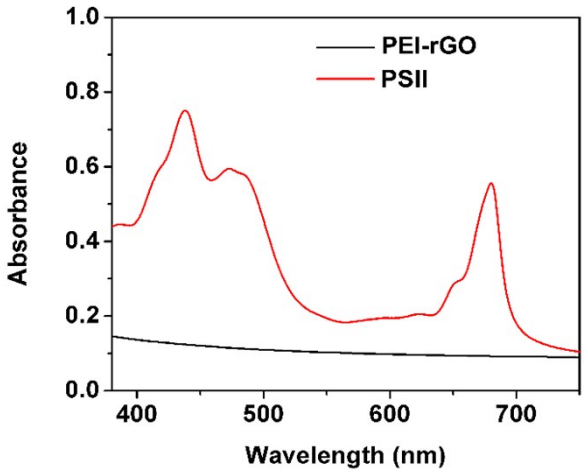

Figure S5. UV-vis spectra of 25 μg mL^{-1} PEI-rGO aqueous dispersion (black curve), and 10 μg Chl mL^{-1} PSII buffer (pH 6.5) suspension (red curve).

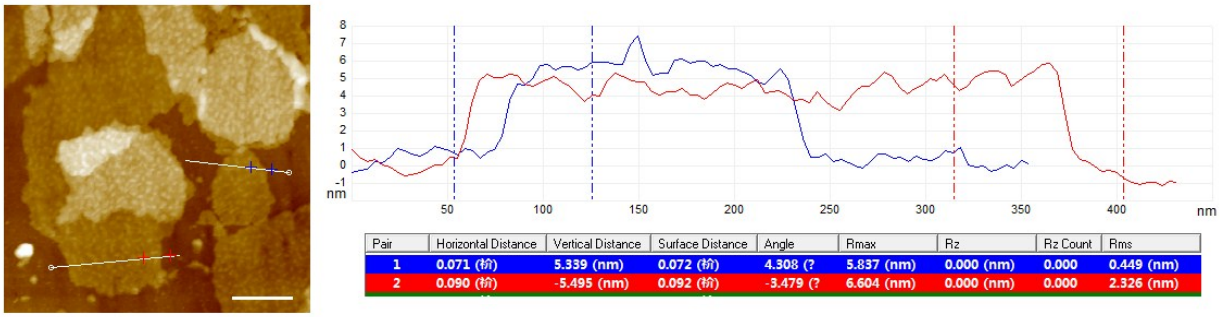

Figure S6. AFM cross-sectional analysis of PSII enriched membranes on silica wafers.

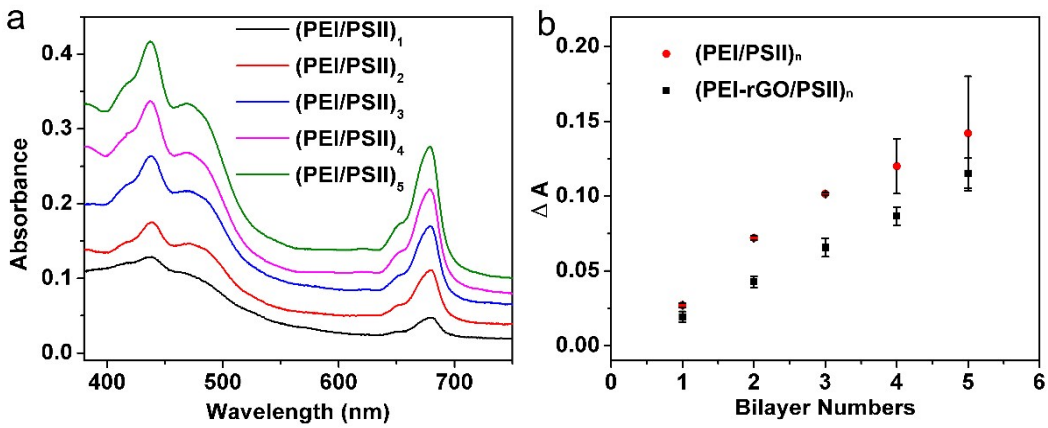

Figure S7. (a) UV-vis spectra of PEI/PSII multilayered films with varying numbers of LbL depositions on ITO substrate. (b) Absorbance difference at 680 and 720 nm of PEI/PSII and PEI-rGO/PSII films on ITO substrate. All data points represent the average of three independent data sets with standard deviation.

A smaller value of PEI-rGO/PSII films is obvious since the surface coverage of PEI-rGO/PSII multilayered films is lower.

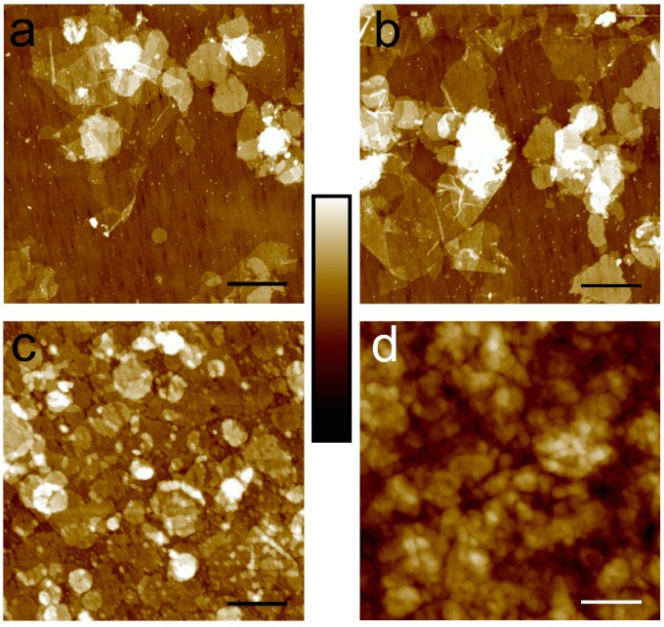

Figure S8. AFM images of (a) $(PEI\text{-}rGO/PSII)_1$, (b) $(PEI\text{-}rGO/PSII)_2$, (c) $(PEI\text{-}rGO/PSII)_3$ and (d) $(PEI/PSII)_3$ multilayered films on ITO substrates. Z-scale bar is 40 nm for (a), (b) and (c), 160 nm for (d), respectively.

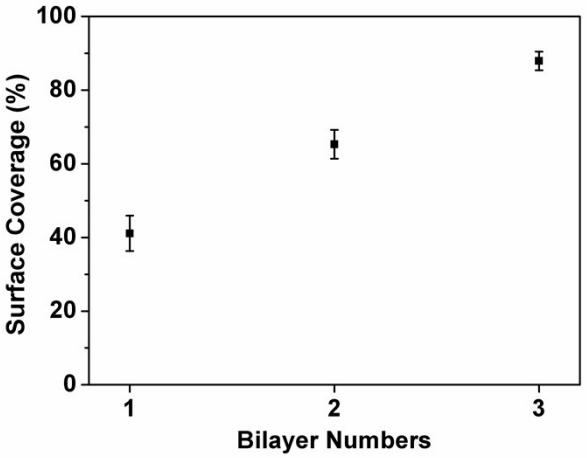

Figure S9. Surface coverage of PEI-rGO/PSII multilayered films. Surface coverage were calculated using ImageJ software by randomly choose five pictures of AFM with areas more than $10 \times 10\ \mu m^2$.

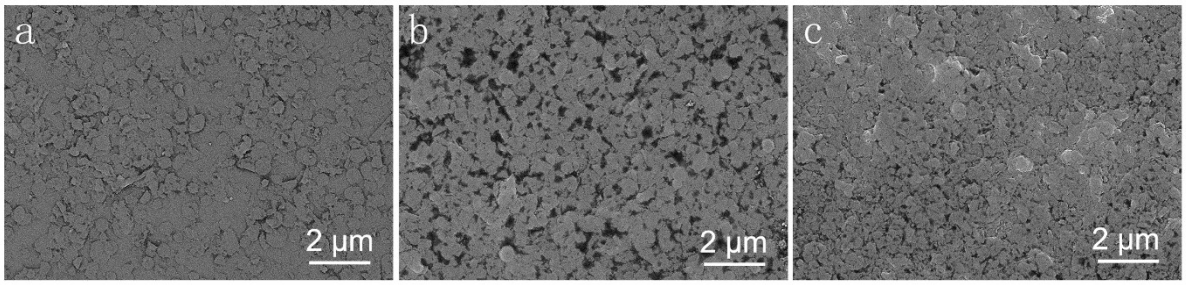

Figure S10. SEM images of (a) $(PEI\text{-}rGO/PSII)_1$; (b) $(PEI\text{-}rGO/PSII)_3$; and (c) $(PEI/PSII)_3$ multilayered films on ITO electrodes.

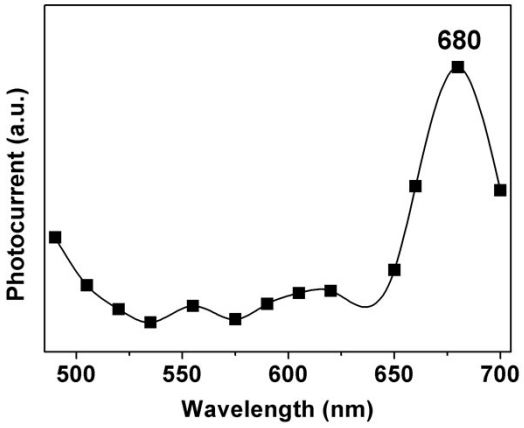

Figure S11. Photocurrent action spectrum of PSII films on ITO substrate.

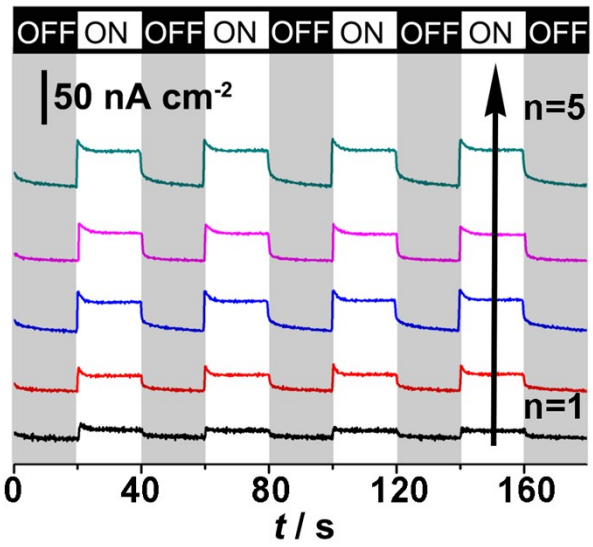

Figure S12. Photocurrent response upon cyclically switched illumination of PEI/PSII multilayered films supported by ITO substrate. The above photocurrents were measured with a bias potential of 0.25 V vs SCE in an aqueous electrolyte buffer solution (pH 6.5, 20 mM MES, 50 mM KCl, 5 mM $MgCl_2$ and 3 mM $CaCl_2$) under light illumination (800 nm > λ > 550 nm, P_{680nm}=10 mW cm^{-2}) at 25 °C.

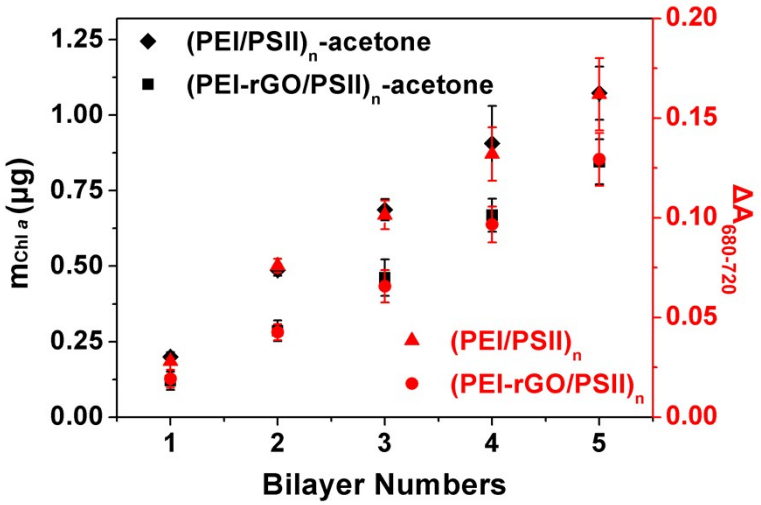

Figure S13. Absorbance difference at 680 and 720 nm of PEI/PSII and PEI-rGO/PSII multilayered films (red point). The mass of Chl *a* in above PEI/PSII and PEI-rGO/PSII multilayered films (black point).

For determining the amount of Chl *a* in each electrode, 80% acetone aqueous solution was used to dissolve the multilayered films. The solution was then measured with UV-vis spectrophotometer. The mass of Chl *a* was calculated using the following equation:

$m_{Chl\ a}$ (μg) = {12.7 × (A_{663} – A_{720}) - 2.59 × (A_{645} – A_{720})} × V(mL)

where m, A and V indicate mass of Chl *a*, absorbance at a certain wavelength and the volume of 80% acetone aqueous solution used for dissolving the films. Taking that multilayered films are assembled on both sides of ITO substrates. The mass used for the calculation of photocurrent generated per μg Chl *a* is divided by two.

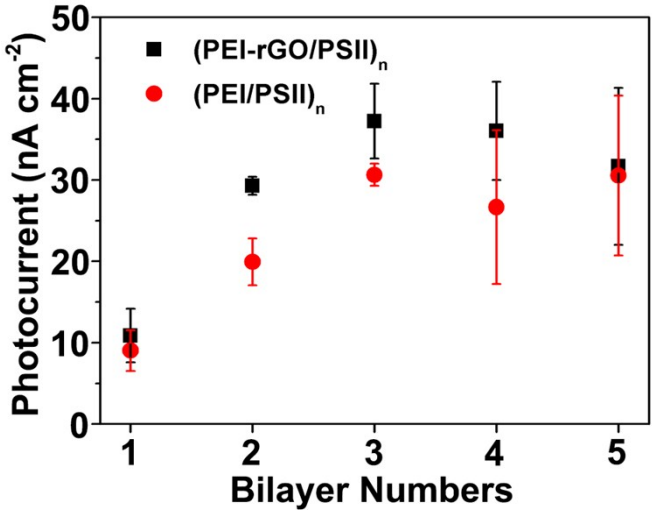

Figure S14. Photocurrent response of PEI-rGO/PSII and PEI/PSII multilayered films as a function of different bilayer numbers. All data points represent the average of three independent data sets with standard deviation.

Table S1 Comparison of PSII-based photoanode systems

Reference	Electrode	PSII source	Light source	Bias voltage (V *vs.* NHE)	DET ($\mu A\ cm^{-2}$)	MET ($\mu A\ cm^{-2}$)	Stability (min)	IPCE (%)[a]	Quantum efficiency (%)
5	mesoITO-PSII	*T. elongatus*	635 nm, 8 mW cm^{-2}	0.50	1.6		$t_{1/2} < 5$		
						12[b]		0.3[b]	
						22[c]			
6	mesoITO-$C_2CO_2^-$-PSII (electrostatic)	*T. elongatus*	679 nm, 10 mW cm^{-2}	0.50	0.28		$t_{1/2} < 5$	0.005	
						1.4[c]		0.03[c]	
6	mesoIT-$C_2CO_2^-$-PSII (covalent)	*T. elongatus*	679 nm, 10 mW cm^{-2}	0.50	0.43		$t_{1/2} \sim 12$	0.01	
						4.5[c]		0.10[c]	
7	Au-Ni-NTA-PSII	*T. vulcanus*	680 nm, 21 mW cm^{-2}	0.40[d]	0.13				
8	Au-pMBQ-PSII	*M. laminosus*	>400 nm, 0.1 W			2.7			1.0
9	Au-Os redox polymer-PSII	T. elongatus	675 nm, 2.65mW cm^{-2}	0.50[e]		45	$t_{0.85} \sim 55$		
This work	ITO-PSII	spinach	800 nm > λ > 550 nm, P_{680nm}=10 mW cm^{-2}	0.49[d]	0.009		$t_{1/2} \sim 19$	0.0002	0.0011
	ITO-$(PEI/PSII)_2$	spinach	800 nm > λ > 550 nm, P_{680nm}=10 mW cm^{-2}	0.49[d]	0.020		$t_{1/2} \sim 20$	0.0004	0.0017
	ITO-$(PEI\text{-}rGO/PSII)_3$	spinach	800 nm > λ > 550 nm, P_{680nm}=10 mW cm^{-2}	0.49[d]	0.037		$t_{1/2} \sim 23$	0.0007	0.0026

[a] IPCE(%) = {1240 × j ($\mu A\ cm^{-2}$)} / {P ($W\ m^{-2}$) × λ (nm)} [b] Mediated electron transfer using 1,4-napthoquinone-2-sulphonate. [c] Mediated electron transfer using 2,6-dichloro-1,4-benzoquinone. [d] Converted from SCE to NHE by the addition of 0.24 V. [e] Converted from Ag/AgCl to NHE by the addition of 0.20 V.

Reference

1 W. S. Hummers and R. E. Offeman, *J. Am. Chem. Soc.*, 1958, **80**, 1339-1339.

2 B. Hankamer, J. Nield, D. Zheleva, E. Boekema, S. Jansson and J. Barber, *Eur. J. Biochem.*, 1997, **243**, 422-429.

3 Y. Yamamoto, J. Leng and J.-R. Shen, in *Photosynthesis Research Protocols*, ed. R. Carpentier, Humana Press, 2011, pp. 1-10.

4 K. K. Rao, D. O. Hall, N. Vlachopoulos, M. Grätzel, M. C. W. Evans and M. Seibert, *J. Photochem. Photobiol. B*, 1990, **5**, 379-389.

5 M. Kato, T. Cardona, A. W. Rutherford and E. Reisner, *J. Am. Chem. Soc.*, 2012, **134**, 8332-8335.

6 M. Kato, T. Cardona, A. W. Rutherford and E. Reisner, *J. Am. Chem. Soc.*, 2013, **135**, 10610-10613.

7 N. Terasaki, M. Iwai, N. Yamamoto, T. Hiraga, S. Yamada and Y. Inoue, *Thin Solid Films*, 2008, **516**, 2553-2557.

8 O. Yehezkeli, R. Tel-Vered, J. Wasserman, A. Trifonov, D. Michaeli, R. Nechushtai and I. Willner, *Nat. Commun*., 2012, **3**, 742.

9 A. Badura, D. Guschin, B. Esper, T. Kothe, S. Neugebauer, W. Schuhmann and M. Rögner, *Electroanalysis*, 2008, **20**, 1043-1047.